Journal of Multi Disciplinary Engineering Technologies
ISSN(P) 0974-1771 ISSN(O) 2581-9372
Volume 19, Issue 02 DOI: https://doi.org/10.64992/jmdet.vol.19.issue.2.13

Generation of Moving Load on an Irregular Fibre Reinforced Half-Space Resting over Ocean using Perturbation Technique

Biru Mandal[1], Rajesh Kumar Tiwari[1], Manoj Kumar singh[2*]

[1]Department of Mathematics, Binod Bihari Mahto Koyalanchal University, Dhanbad, 826004, Jharkhand, India.
[2]P.G. Department of Mathematics, Magadh University, Bodh Gaya, 824234, Bihar, India.

*Corresponding author(s). E-mail(s): manojmathism@gmail.com;
Contributing authors: mandalbiru7@gmail.com; rk5671417@gmail.com;

Abstract

Significant stresses and progressive deformation in civil engineering and fracture mechanics structures may result from the development of dynamic loads brought on by heavy vehicle traffic and seismic disturbances in bridge construction areas. Investigating the impact of different factors related to moving loads acting on rock media sitting over a water medium is therefore crucial. The practical importance of the current study is established by the observation of huge rock formations atop water-supported foundations in various oceanic zones. In this work, the framework of geophysical fracture mechanics has been used to analyze the stress produced by a moving load acting on a fiber-reinforced rock medium. Examining the stresses caused by a normal moving load acting on the free surface of an uneven fiber-reinforced rock layer sitting on a water medium is the study's primary goal. Three distinct kinds of surface imperfections have been examined and visually explained. Additionally, pictorial representations have been used to highlight a number of significant physical traits linked to stress behavior.

Keywords: Normal and shear stress, parabolic and rectangular irregularity, Perturbation Technique

1 Introduction

In its most basic form, horizontal layering shows that the Earth's material has a vertical axis of symmetry and is transversely isotropic, meaning that its elastic characteristics change vertically while remaining constant horizontally. The dynamic marine environment produces a variety of stresses that affect the behavior of rocks and other solid materials

Received 23 March 2026; Revised 23 May 2026; Accepted 13 July 2026; Available online 20 July 2026

resting on the ocean floor. The Earth, which is made up of silicate and iron alloy components, is frequently modelled as a multilayered medium with layers of varying density and stiffness properties. These stressors can be caused by a variety of factors, including sediment movement, wave activity, ocean currents, and water pressure. In geomechanics, the impact of moving load on an irregular surface is an inspiring topic to study for all seismologist and civil engineers due to its extensive application in different medium of transport engineering containing project designing of construction of railways track, tunnels and bridges. Cole and Huth [1], Craggs [2], Sneddon [3] and Cole and Huth [4] examined the stress induced raised by but he employed a different approach to solving it. Past researchers have provided notable investigation of single layered problem applied to moving load with consideration of different irregularity induced by vehicles movement. Therefore, studying the dynamic behavior of a transversely isotropic material under moving loads may be helpful for design and construction applications. Furthermore, because the Earth's crust is often full of flaws of various sizes and shapes, rocks are rarely uniform in nature. Rocks become weaker due to weathering, erosion, and other external influences, which can significantly raise the risk of buildings like railroad bridges collapsing under high-speed trains. Moreover, some authors have discussed problems involving single-layered structures, including Singh et al. ([5] and [6]). Further elaboration of the subject is provided in the studies by [7], [8], [9], [10] and [11]) In geomechanics, the impact of moving load on an irregular surface is an inspiring topic to study for all seismologist and civil engineers due to its extensive application in different medium of transport engineering containing project designing of construction of railways track, tunnels and bridges. Furthermore, rocks are rarely homogeneous in nature since the Earth's crust is frequently filled with imperfections of different sizes and shapes. Weathering, erosion, and external factors cause a variety of irregularity in rocks that weaken them and can greatly increase the likelihood that structures like railway bridges would collapse under high-speed trains Analysis of surface waves in irregular media and sliding interface is discussed by many authors including [12]- [13]. Many researchers have contributed their research work based on moving load but their research work was limited to single medium problem but in real situation it is found that moving load is happening in doubly layered problem also. The combined effects of moving loads along with Hydrostatic stress in three-dimensional having double-layered structures, have not been thoroughly examined. This gap in the literature will be addressed in the current model to enable more comprehensive studies of moving load interactions in complex, real-world structural systems under moving load. The behavior of many composite materials reinforced with elastic fiber is very anisotropic. Fiber-reinforced materials are characterized by their components acting. When faced with an issue, it is crucial to consider the irregularities of the Earth's crust, which are generally irregular in size and shape. An intriguing mechanical problem with applications to the medium's stability is the stress generated in the body as a result of a moving load causing fracture. Because it may be useful in estimating a structure's strength, the reaction of a moving load across a surface is being studied. Recently, Stress generated due to moving load on orthotropic gravitational elastic plate and porous composite rock structure [14]- [15]. However, the fact that various rocks float in the water motivates the current problem, which has a real-world application, whereas earlier works were unrelated. This study examines how the stress distribution caused by a load traveling at a constant speed along the upper free surface of a rock medium resting over the ocean is affected by a number of factors, including depth, material heterogeneity, maximum irregularity depth, and rock layer thickness. The analysis takes the medium's exponential heterogeneity into

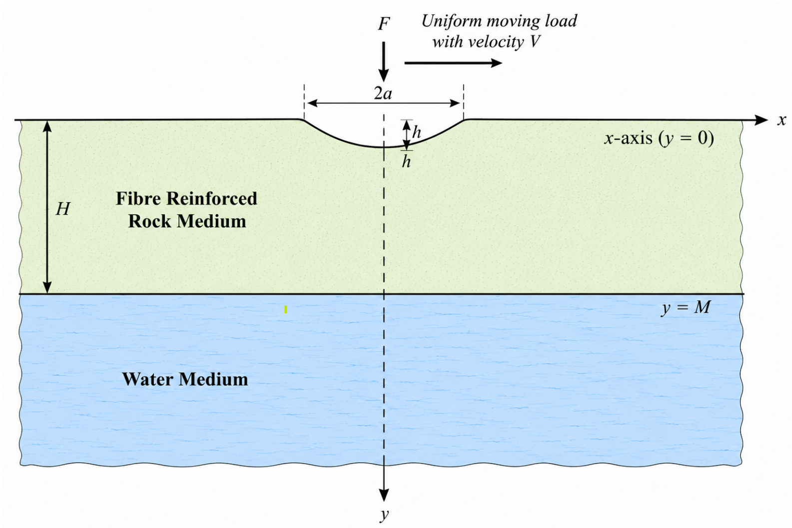

Fig. 1: Geometry of the Problem

account. For the upper and lower media, closed-form equations for tangential and normal stresses are obtained. Graphical representations are used to investigate and comprehend various surface irregularity scenarios, such as parabolic, rectangular, and no irregularity. Additionally, the effects of the indicated parameters are assessed by numerical simulations, and the resulting stress distributions are graphically depicted. The results are contrasted with actual geological conditions found in the crust of the Earth, showing.

2 Formulation of Problem

We consider a model consisting of a transversely isotropic layer of thickness H with an irregular surface. The surface irregularity is assumed to have a parabolic profile with width a_1 and depth h_1. A rectangular coordinate system is chosen such that the origin O is located at the midpoint of the span $2a$ of the irregularity. As shown in Fig. 1, the y-axis is directed vertically downward into the layer, while a load F moves with a constant velocity v along the x-axis on the surface. The plane $y = M$ represents the surface of the water medium. The analysis is restricted to two-dimensional motion in the x–y plane.

The equation describing the surface irregularity is given by

$$y = \epsilon f(x), \tag{1}$$

where $f(x)$ denotes the shape function representing the parabolic irregularity and is defined as

$$f(x) = \begin{cases} 0, & |x| \geq a, \\ \dfrac{2}{a}\left(a^2 - x^2\right), & |x| \leq a. \end{cases} \tag{2}$$

The perturbation parameter ϵ is assumed to be extremely small and is defined as

$$\epsilon = \frac{h}{2a}, \tag{3}$$

where h is the depth of the irregularity and $2a$ is its span. It is assumed that the depth of the irregularity is much smaller than its span, i.e.,

$$\frac{h}{2a} \ll 1, \tag{4}$$

which implies that

$$\epsilon \ll 1. \tag{5}$$

This assumption justifies the use of perturbation techniques and linearized boundary conditions, thereby enabling an analytical treatment of the governing equations for stress and deformation in the heterogeneous transversely isotropic medium.

2.1 Mathematical formulations for Upper fibre-reinforced rock medium

The constitutive relation between stress and strain for a fiber-reinforced elastic material with preferred reinforcement direction $\hat{\mathbf{a}}$ (Belfield *et al.* [**?**]) is given by

$$\begin{aligned} S_{ij} = \lambda \hat{e}_{kk}\delta_{ij} + 2\mu_T \hat{e}_{ij} + \alpha\left(\hat{a}_k\hat{a}_m\hat{e}_{km}\delta_{ij} + \hat{e}_{kk}\hat{a}_i\hat{a}_j\right) \\ + 2(\mu_L - \mu_T)\left(\hat{a}_i\hat{a}_k\hat{e}_{kj} + \hat{a}_j\hat{a}_k\hat{e}_{ki}\right) + \beta\hat{a}_k\hat{a}_m\hat{e}_{km}\hat{a}_i\hat{a}_j, \end{aligned} \tag{6}$$

where $i, j, k, m = 1, 2, 3$, S_{ij} and

$$\hat{e}_{ij} = \frac{1}{2}\left(u_{i,j} + u_{j,i}\right)$$

denote the stress and strain components, respectively. Here, δ_{ij} is the Kronecker delta and

$$\hat{\mathbf{a}} = (a_1, a_2, a_3)$$

represents the preferred direction of reinforcement. The elastic constants λ, μ_T, μ_L, α, and β characterize the anisotropic response of the fiber-reinforced material, where μ_L and μ_T denote the longitudinal and transverse shear moduli, respectively.

For the present configuration, the stress components reduce to

$$S_{11} = (\lambda + 2\alpha + 4\mu_L - 2\mu_T + \beta)\,\hat{e}_{11} + (\lambda + \alpha)\hat{e}_{22} + (\lambda + \alpha)\hat{e}_{33}, \tag{7}$$

$$S_{22} = (\lambda + \alpha)\hat{e}_{11} + (\lambda + 2\mu_T)\hat{e}_{22} + \lambda\hat{e}_{33}, \tag{8}$$

$$S_{33} = (\lambda + \alpha)\hat{e}_{11} + \lambda\hat{e}_{22} + (\lambda + 2\mu_T)\hat{e}_{33}, \tag{9}$$

and

$$S_{23} = 2\mu_T\hat{e}_{23}, \qquad S_{13} = 2\mu_L\hat{e}_{13}, \qquad S_{12} = 2\mu_L\hat{e}_{12}. \tag{10}$$

The equations of motion for the fiber-reinforced medium are

$$\frac{\partial S_{11}}{\partial x} + \frac{\partial S_{12}}{\partial y} = \rho_1\frac{\partial^2 u_1}{\partial t^2}, \tag{11}$$

$$\frac{\partial S_{21}}{\partial x} + \frac{\partial S_{22}}{\partial y} = \rho_1\frac{\partial^2 v_1}{\partial t^2}. \tag{12}$$

Substituting Eqs. (7)–(10) into Eqs. (11) and (12) yields

$$
\begin{aligned}
&(\lambda + 2\alpha + 4\mu_L - 2\mu_T + \beta)\,\frac{\partial^2 u_1}{\partial x^2} + (\lambda + \alpha + \mu_L)\frac{\partial^2 v_1}{\partial x \partial y} \\
&\quad + \mu_L \frac{\partial^2 u_1}{\partial y^2} = \rho_1 \frac{\partial^2 u_1}{\partial t^2}.
\end{aligned} \tag{13}
$$

$$
\mu_L \frac{\partial^2 v_1}{\partial x^2} + (\lambda + \alpha + \mu_L)\frac{\partial^2 u_1}{\partial x \partial y} + (\lambda + 2\mu_T)\frac{\partial^2 v_1}{\partial y^2} = \rho_1 \frac{\partial^2 v_1}{\partial t^2}. \tag{14}
$$

The solutions of Eqs. (13) and (14) are assumed in the form

$$
u_1 = \int_0^\infty A_1 e^{-kqy} \cos k(x - Vt)\, dk, \tag{15}
$$

$$
v_1 = \int_0^\infty A_2 e^{-kqy} \sin k(x - Vt)\, dk, \tag{16}
$$

where k is the wave number, V is the velocity of the moving load, t denotes time, q is an unknown positive dimensionless parameter independent of k, and A_1 and A_2 are arbitrary constants. The parameter q is chosen so that the displacement field remains bounded as $y \to \infty$.

Substitution of Eqs. (15) and (16) into the governing equations yields

$$
A_1 \left[\lambda + 2\alpha + 4\mu_L - 2\mu_T + \beta - \mu_L q^2 - \rho_1 V^2\right] + A_2(\lambda + \alpha + \mu_L)q = 0, \tag{17}
$$

$$
A_1(\lambda + \alpha + \mu_L)q + A_2\left[(\lambda + 2\mu_T)q^2 - \mu_L + \rho_1 V^2\right] = 0. \tag{18}
$$

The consistency condition of Eqs. (17) and (18) gives

$$
q^4 + B_1 q^2 + C_1 = 0, \tag{19}
$$

where

$$
B_1 = \frac{\rho_1 V^2 - \mu_L}{\lambda + 2\mu_T} + \frac{\rho_1 V^2 - (\lambda + 2\alpha + 4\mu_L - 2\mu_T + \beta)}{\mu_L} + \frac{(\lambda + \alpha + \mu_L)^2}{\mu_L(\lambda + 2\mu_T)}, \tag{20}
$$

and

$$
C_1 = \frac{(\rho_1 V^2 - \mu_L)\left[\rho_1 V^2 - (\lambda + 2\alpha + 4\mu_L - 2\mu_T + \beta)\right]}{\mu_L(\lambda + 2\mu_T)}. \tag{21}
$$

The roots are

$$
q_i^2 = \frac{-B_1 \pm \sqrt{B_1^2 - 4C_1}}{2}, \qquad i = 1, 2. \tag{22}
$$

For q_1 and q_2 to be real, both q_1^2 and q_2^2 must be positive. This requires

$$
(\rho_1 V^2 - \mu_L)\left[\rho_1 V^2 - (\lambda + 2\alpha + 4\mu_L - 2\mu_T + \beta)\right] > 0,
$$

which implies

$$
V > \sqrt{\frac{\mu_L}{\rho_1}}, \qquad V > \sqrt{\frac{\lambda + 2\alpha + 4\mu_L - 2\mu_T + \beta}{\rho_1}}.
$$

Hence, the displacement field can be expressed as

$$u_1 = \int_0^\infty \left[A_1 e^{-kq_1 y} + A_2 e^{-kq_2 y}\right] \cos k(x - Vt)\, dk, \tag{23}$$

and

$$v_1 = \int_0^\infty \left[A_1 \delta_1 e^{-kq_1 y} + A_2 \delta_2 e^{-kq_2 y}\right] \sin k(x - Vt)\, dk, \tag{24}$$

where

$$\delta_1 = \frac{\mu_L q_1^2 + \rho_1 V^2 - (\lambda + 2\alpha + 4\mu_L - 2\mu_T + \beta)}{(\lambda + \alpha + \mu_L) q_1}, \tag{25}$$

$$\delta_2 = \frac{\mu_L q_2^2 + \rho_1 V^2 - (\lambda + 2\alpha + 4\mu_L - 2\mu_T + \beta)}{(\lambda + \alpha + \mu_L) q_2}. \tag{26}$$

2.2 Solution in case of lower half-space

The constitutive relation for the lower half-space is given by

$$(\tau_{ij})_2 = \eta \Delta \delta_{ij} + 2\mu \omega_{ij}, \tag{27}$$

where η and μ are the Lamé constants, δ_{ij} is the Kronecker delta, ω_{ij} denotes the strain tensor, and Δ is the dilatation.

Accordingly, the equations of motion for the lower half-space under hydrostatic stress are

$$(\eta + \mu) \frac{\partial \Delta}{\partial x} + \mu \nabla^2 u_2 - \beta \nabla^2 u_2 = \rho_2 \frac{\partial^2 u_2}{\partial t^2}, \tag{28}$$

$$(\eta + \mu) \frac{\partial \Delta}{\partial z} + \mu \nabla^2 v_2 - \beta \nabla^2 v_2 = \rho_2 \frac{\partial^2 v_2}{\partial t^2}, \tag{29}$$

where

$$\nabla^2 = \frac{\partial^2}{\partial x^2} + \frac{\partial^2}{\partial z^2}. \tag{30}$$

Since the lower medium is assumed to be a fluid, the shear modulus vanishes ($\mu = 0$). Therefore, Eqs. (28) and (29) reduce to

$$(\eta - \beta) \frac{\partial^2 u_2}{\partial x^2} + \eta \frac{\partial^2 v_2}{\partial x \partial z} - \beta \frac{\partial^2 u_2}{\partial z^2} = \rho_2 \frac{\partial^2 u_2}{\partial t^2}, \tag{31}$$

$$(\eta - \beta) \frac{\partial^2 v_2}{\partial z^2} + \eta \frac{\partial^2 u_2}{\partial x \partial z} - \beta \frac{\partial^2 v_2}{\partial x^2} = \rho_2 \frac{\partial^2 v_2}{\partial t^2}. \tag{32}$$

Introducing the displacement potential ψ_2 such that

$$u_2 = \frac{\partial \psi_2}{\partial x}, \qquad v_2 = \frac{\partial \psi_2}{\partial z},$$

Eqs. (31) and (32) reduce to

$$\frac{\partial^2 \psi_2}{\partial x^2} + \frac{\partial^2 \psi_2}{\partial z^2} = \frac{1}{\beta_2^2} \frac{\partial^2 \psi_2}{\partial t^2}, \tag{33}$$

where

$$\beta_2 = \sqrt{\frac{\eta - \beta}{\rho_2}}. \tag{34}$$

The solution of Eq. (33) is assumed in the form

$$\psi_2(x,z,t) = \int_0^\infty G e^{-kq_3 z} \cos k(x - Vt)\, dk, \tag{35}$$

where

$$q_3 = \sqrt{1 - \left(\frac{V}{\beta_2}\right)^2}. \tag{36}$$

Consequently, the displacement components of the lower half-space become

$$u_2 = -k \int_0^\infty G e^{-kq_3 z} \sin k(x - Vt)\, dk, \tag{37}$$

$$v_2 = -kq_3 \int_0^\infty G e^{-kq_3 z} \cos k(x - Vt)\, dk. \tag{38}$$

2.3 Boundary Conditions

The boundary conditions at the irregular interface are

$$(S_{12})_1 - \epsilon h'(x)(S_{22})_1 = 0, \tag{39}$$

$$(S_{11})_1 - \epsilon h'(x)(S_{12})_1 = -F\delta(x - Vt), \tag{40}$$

where

$$\delta(x - Vt) = \frac{1}{\pi} \int_0^\infty \cos k(x - Vt)\, dk, \tag{41}$$

is the Dirac delta function.

At the interface, continuity conditions require

$$u_1 = u_2, \qquad v_1 = v_2, \qquad (S_{22})_1 = (\tau_{22})_2, \qquad (S_{12})_1 = (\tau_{12})_2. \tag{42}$$

The stress components are

$$(S_{22})_1 = (\lambda + \alpha)\frac{\partial u_1}{\partial x} + (\lambda + 2\mu_T)\frac{\partial v_1}{\partial y}, \tag{43}$$

$$(S_{12})_1 = \mu_L \left(\frac{\partial u_1}{\partial y} + \frac{\partial v_1}{\partial x}\right). \tag{44}$$

The unknown coefficients are expanded in powers of the perturbation parameter ϵ as (Kaur and Singh [16])

$$A_1 \simeq A_{10} + A_{11}\epsilon, \qquad A_2 \simeq A_{20} + A_{21}\epsilon. \tag{45}$$

Since q_1, q_2, δ_1 and δ_2 are independent of k, the displacement components become

$$
\begin{aligned}
u_1 = \int_0^\infty \Big[(A_{10} + A_{11}\epsilon)e^{-kq_1y} \\
+ (A_{20} + A_{21}\epsilon)e^{-kq_2y}\Big] \cos k(x - Vt)\, dk.
\end{aligned} \tag{46}
$$

$$
\begin{aligned}
v_1 = \int_0^\infty \Big[(A_{10} + A_{11}\epsilon)\delta_1 e^{-kq_1y} \\
+ (A_{20} + A_{21}\epsilon)\delta_2 e^{-kq_2y}\Big] \sin k(x - Vt)\, dk.
\end{aligned} \tag{47}
$$

Substituting Eqs. (46) and (47) into the boundary conditions yields the following system of linear equations:

$$
[(\lambda + \alpha) + \delta_1 q_1(\lambda + 2\mu_T)]\, A_{10} + [(\lambda + \alpha) + \delta_2 q_2(\lambda + 2\mu_T)]\, A_{20} = 0, \tag{48}
$$

$$
\begin{aligned}
&[(\lambda + \alpha) + \delta_1 q_1(\lambda + 2\mu_T)]\, A_{11} \\
&+ [(\lambda + \alpha) + \delta_2 q_2(\lambda + 2\mu_T)]\, A_{21} \\
&- \big[kq_1h(\lambda + \alpha) - kq_1^2h\delta_1(\lambda + 2\mu_T)\big]\, A_{10} \\
&+ \big[kq_2h(\lambda + \alpha) - kq_2^2h\delta_2(\lambda + 2\mu_T)\big]\, A_{20} = 0.
\end{aligned} \tag{49}
$$

$$
(\delta_1 - q_1)A_{10} + (\delta_2 - q_2)A_{20} = -\frac{F}{\pi k\mu_L}, \tag{50}
$$

$$
\begin{aligned}
&(\delta_1 - q_1)A_{11} + (\delta_2 - q_2)A_{21} \\
&+ (kq_1^2h - \delta_1 q_1 kh)A_{10} + (kq_2^2h - \delta_2 q_2 kh)A_{20} = 0.
\end{aligned} \tag{51}
$$

Solving Eqs. (48)–(51), we obtain

$$
A_{10} = \frac{(\mathcal{E} + \delta_2 q_2\mathcal{Z})D}{k}, \qquad A_{20} = -\frac{(\mathcal{E} + \delta_1 q_1\mathcal{Z})D}{k}, \tag{52}
$$

$$
A_{11} = \frac{\mathcal{E}_1(\delta_2 - q_2) - \mathcal{E}_2(\mathcal{E} + \delta_1 q_1\mathcal{Z})}{k}\left(\frac{D\pi\mu_L}{F}\right), \tag{53}
$$

$$
A_{21} = \frac{\mathcal{E}_2(\mathcal{E} + \delta_1 q_1\mathcal{Z}) - \mathcal{E}_1(\delta_1 - q_1)}{k}\left(\frac{D\pi\mu_L}{F}\right). \tag{54}
$$

where

$$
\mathcal{E} = \lambda + \alpha, \qquad \mathcal{Z} = \lambda + 2\mu_T, \tag{55}
$$

$$
D = -\frac{F}{\pi\mu_L\left[(\mathcal{E} + \delta_2 q_2\mathcal{Z})(\delta_2 - q_2) - (\delta_1 - q_1)(\mathcal{E} + \delta_1 q_1\mathcal{Z})\right]}, \tag{56}
$$

$$
\mathcal{E}_1 = (\mathcal{E} + \delta_2 q_2\mathcal{Z})(\mathcal{E} + \delta_1 q_1\mathcal{Z})(q_1 - q_2)hD, \tag{57}
$$

$$
\mathcal{E}_2 = \left[(\mathcal{E} + \delta_1 q_1\mathcal{Z})(q_2 - \delta_2)q_2 - (\mathcal{E} + \delta_2 q_2\mathcal{Z})(q_1 - \delta_1)q_1\right] hD. \tag{58}
$$

The non-vanishing stress components are obtained as (Kaur and Singh [**?**])

$$
S_{11} = -\frac{D(\mathcal{E} + \delta_2 q_2\mathcal{Z})\left[(\lambda + 2\alpha + 4\mu_L - 2\mu_T + \beta) + \delta_1 q_1\mathcal{E}\right]}{q_1^2y^2 + (x - Vt)^2}
$$

$$
\begin{aligned}
&+\frac{D(\mathcal{E}+\delta_1 q_1 \mathcal{Z})\left[(\lambda+2\alpha+4\mu_L-2\mu_T+\beta)+\delta_2 q_2\mathcal{E}\right]}{q_2^2y^2+(x-Vt)^2}\\
&+2\epsilon(x-Vt)\left[\frac{q_1 y\left[-(\lambda+2\alpha+4\mu_L-2\mu_T+\beta)-\delta_1 q_1\mathcal{E}\right]}{\left[q_1^2y^2+(x-Vt)^2\right]^2}\right.\\
&\left.+\frac{q_2 y\left[(\lambda+2\alpha+4\mu_L-2\mu_T+\beta)+\delta_1 q_1\mathcal{E}\right]D\pi\mu_L}{kF\left[q_2^2y^2+(x-Vt)^2\right]^2\left[\mathcal{E}_2(\mathcal{E}+\delta_1 q_1\mathcal{Z})-\mathcal{E}_1(\delta_1-q_1)\right]}\right]. \quad (59)
\end{aligned}
$$

$$
\begin{aligned}
S_{22}=&\frac{D(\mathcal{E}+\delta_2 q_2\mathcal{Z})(\mathcal{E}+\delta_1 q_1\mathcal{Z})}{q_1^2y^2+(x-Vt)^2}\\
&+\frac{D(\mathcal{E}+\delta_1 q_1\mathcal{Z})(\mathcal{E}+\delta_2 q_2\mathcal{Z})}{q_2^2y^2+(x-Vt)^2}\\
&+2\epsilon(x-Vt)\left[\frac{q_1 y\left[\mathcal{E}_1(\delta_2-q_2)-\mathcal{E}_2(\mathcal{E}+\delta_1 q_1\mathcal{Z})\right]}{\left[q_1^2y^2+(x-Vt)^2\right]^2}\frac{D\pi\mu_L}{kF}\right.\\
&\left.+\frac{q_2 y\left[\mathcal{E}_2(\mathcal{E}+\delta_1 q_1\mathcal{Z})-\mathcal{E}_1(\delta_1-q_1)\right]}{\left[q_2^2y^2+(x-Vt)^2\right]^2}\frac{D\pi\mu_L}{kF}\right]. \quad (60)
\end{aligned}
$$

$$
\begin{aligned}
S_{12}=&\frac{q_1 y D(\mathcal{E}+\delta_2 q_2\mathcal{Z})(\delta_1-q_1)}{q_1^2y^2+(x-Vt)^2}\\
&+\frac{q_2 y D(\mathcal{E}+\delta_2 q_2\mathcal{Z})(q_2-\delta_2)}{q_2^2y^2+(x-Vt)^2}\\
&+\epsilon\mu_L\left[\frac{q_1 y\left[\mathcal{E}_1(\delta_2-q_2)-\mathcal{E}_2(\mathcal{E}+\delta_1 q_1\mathcal{Z})\right]}{\left[q_1^2y^2+(x-Vt)^2\right]^2}\frac{(y^2+(x-Vt)^2)D\pi\mu_L}{kF}\right.\\
&\left.+\frac{q_2 y(q_2^2y^2-(x-Vt)^2)\left[\mathcal{E}_2(\mathcal{E}+\delta_1 q_1\mathcal{Z})-\mathcal{E}_1(\delta_1-q_1)\right]}{\left[q_2^2y^2+(x-Vt)^2\right]^2}\frac{D\pi\mu_L}{kF}\right]. \quad (61)
\end{aligned}
$$

The normal stress in the lower half-space is

$$
\frac{\tau_{22}}{F}=\frac{\lambda q_3(q_3^2-1)k^2y}{q_3^2y^2+(x-Vt)^2}\,G, \quad (62)
$$

where

$$
\begin{aligned}
G=\frac{q_3^2N^2+(x-Vt)^2}{\eta q_3 kN(q_3^2-1)}&\left[\left(\frac{\mathcal{C}_{33}^0 q_1 n_1-\mathcal{C}_{13}^0}{q_1^2N^2+(x-Vt)^2}+\frac{\mathcal{C}_{33}^0 q_2 n_2-\mathcal{C}_{13}^0}{q_2^2N^2+(x-Vt)^2}\right)(x-Vt)\right.\\
&\left.-\left(\frac{(\mathcal{C}_{33}^0 q_1 n_1-\mathcal{C}_{13}^0)q_1}{q_1^2N^2+(x-Vt)^2}+\frac{(\mathcal{C}_{33}^0 q_2 n_2-\mathcal{C}_{13}^0)q_2}{q_2^2N^2+(x-Vt)^2}\right)N\right]. \quad (63)
\end{aligned}
$$

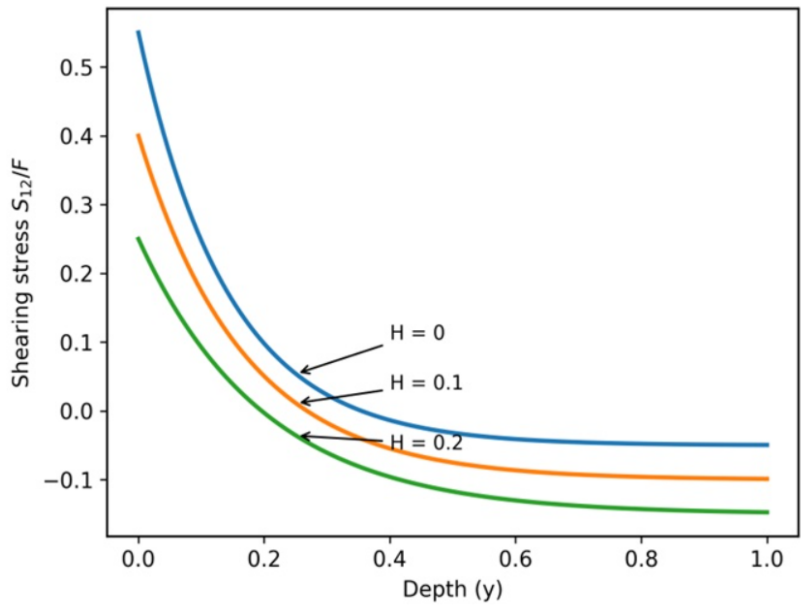

Fig. 2: Plot of the normalized shear stress, S_{12}/F, in the upper medium as a function of depth y for different values of the applied load F and layer thickness H.

3 Numerical results and discussions

The numerical computations are carried out using the following material properties.

For the fiber-reinforced rock medium [**?**],

$$\begin{aligned} \mu_L &= 5.66 \times 10^9 \ \mathrm{N\,m^{-2}}, \\ \mu_T &= 2.46 \times 10^9 \ \mathrm{N\,m^{-2}}, \\ \lambda &= 5.65 \times 10^9 \ \mathrm{N\,m^{-2}}, \\ \alpha &= -1.28, \\ \beta &= 220.90 \times 10^9 \ \mathrm{N\,m^{-2}}, \\ \rho_1 &= 7800 \ \mathrm{kg\,m^{-3}}. \end{aligned} \tag{64}$$

For the water medium (Ewing *et al.* [**?**]),

$$\begin{aligned} \lambda_2 &= 0.214 \times 10^9 \ \mathrm{N\,m^{-2}}, \\ \rho_2 &= 1.0 \times 10^3 \ \mathrm{kg\,m^{-3}}. \end{aligned} \tag{65}$$

Figures 2 and 3 illustrate the variation of the normalized shear stress, S_{12}/F, and the normalized normal stress, S_{22}/F, in the upper medium with respect to the depth coordinate y for different values of the irregularity depth H. It is observed that both the normal and shear stresses decrease with increasing depth, indicating that depth has a significant influence on the stress distribution. The first curve corresponds to the case of a regular surface ($H = 0$), whereas the remaining curves represent different irregular surface profiles. The results further reveal that the stress magnitudes are comparatively higher for the regular surface than for the irregular surfaces, demonstrating that surface irregularity reduces the stress concentration within the medium.

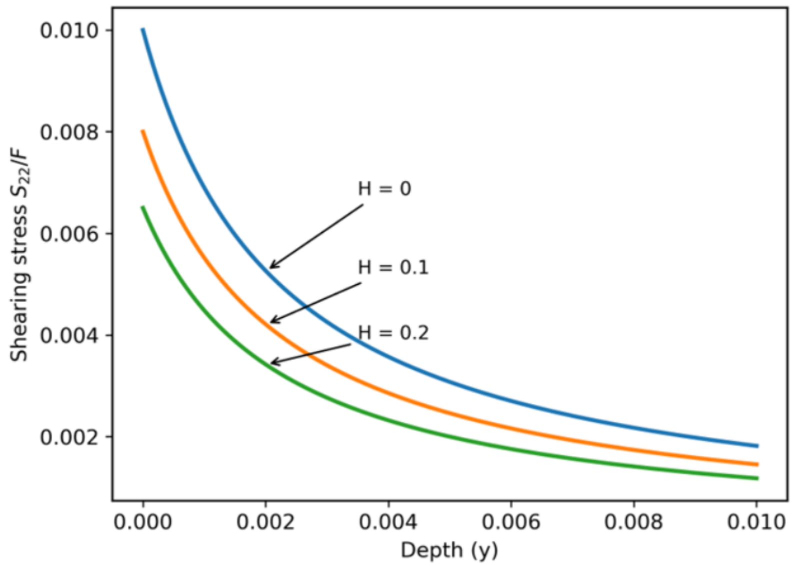

Fig. 3: Plot of the normalized normal stress, S_{22}/F, versus the depth coordinate y for different values of the irregularity depth H.

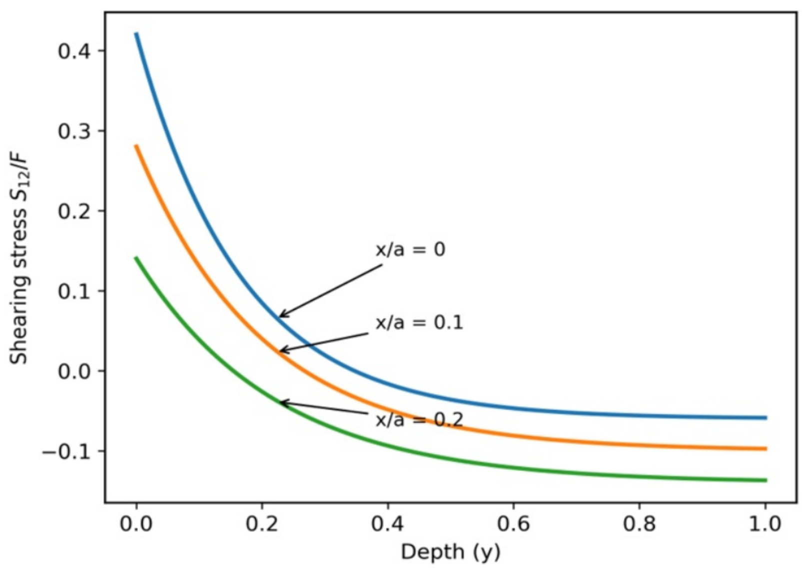

Fig. 4: Plot of the normalized shear stress, S_{12}/F, versus the depth coordinate y for various values of the applied load F in the case of parabolic irregularities $(x/a = 0.1,\ 0.2)$ and a rectangular irregularity $(x/a = 0)$.

Figures 4 and 5 illustrate the influence of parabolic irregularities $(x/a = 0.1,\ 0.2)$ and a rectangular irregularity $(x/a = 0)$ on the stress distribution in the upper medium. The results show that both the normalized normal stress, S_{22}/F, and the normalized shear stress, S_{12}/F, decrease with increasing depth parameter y. It is further observed that surface irregularity reduces the magnitude of the generated stresses. A comparison of the stress profiles indicates that the rectangular irregularity produces comparatively higher

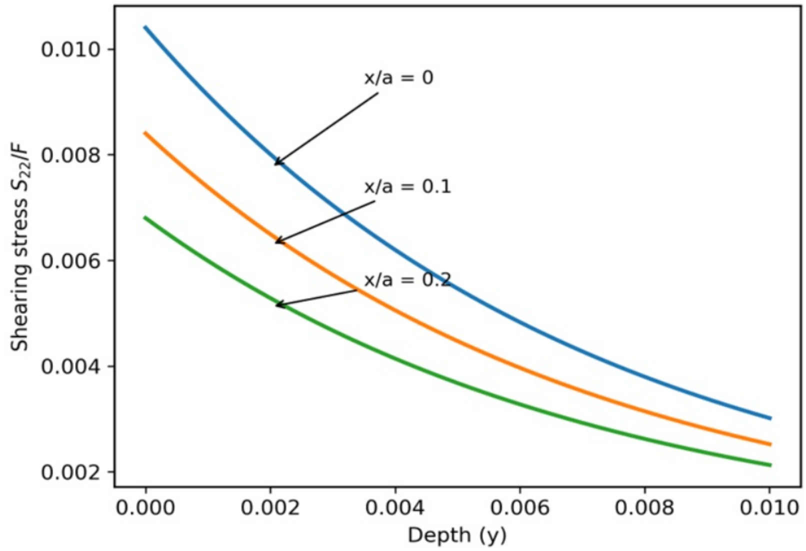

Fig. 5: Plot of the normalized normal stress, S_{22}/F, versus the depth coordinate y for different surface profiles, including parabolic irregularities ($x/a = 0.1,\ 0.2$) and a rectangular irregularity ($x/a = 0$).

stresses than the parabolic irregularity, demonstrating the significant influence of surface geometry on the stress distribution.

Figure 6 illustrates the variation of the normalized stress components with depth for different values of the dimensionless wave number, $kH = 0.1,\ 0.2$, and 0.3. The results indicate that an increase in the wave number leads to a corresponding increase in the magnitude of the induced stresses in the upper medium.

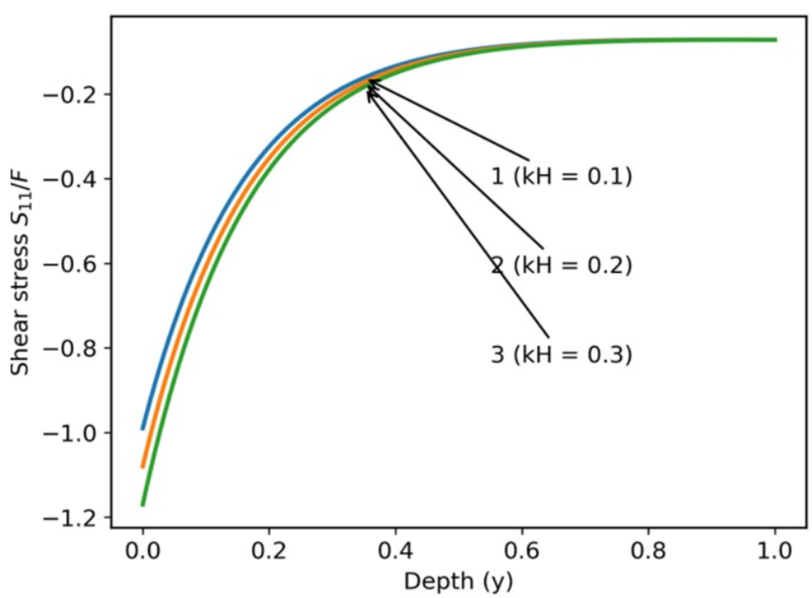

Fig. 6: Plot of the normalized normal stress, S_{11}/F, versus the depth coordinate y for different values of the dimensionless wave number, $kH = 0.1,\ 0.2$, and 0.3.

Overall, the graphical results demonstrate that although a larger wave number enhances the induced stresses, both the normalized normal and shear stresses decrease with increasing depth and surface irregularity. Furthermore, the stress distribution is significantly influenced by the geometry of the surface irregularity, with the rectangular irregularity producing comparatively higher stress magnitudes than the parabolic irregularity. These findings provide valuable insights into the stress behavior of fiber-reinforced geological media subjected to moving loads and have potential applications in the design and analysis of tunnel linings, bridge foundations, underground transportation systems, and earthquake-resistant geotechnical structures.

4 Conclusion

The stresses caused by a moving load acting on an uneven fiber-reinforced rock medium sitting on a water medium are examined in the current work. Three types of surface configurations, namely rectangular, parabolic, and no irregularity, have been investigated. The analytical solution of the governing equations has been obtained by using the perturbation method. Depth has adverse effect on normal and shear stresses, i.e., as depth increases shear stress decrease. Both normal and shear stresses drop with increasing depth, according to the graphical analysis, demonstrating the negative impact of the depth parameter on stress propagation. Additionally, the irregularity factor and irregularity depth parameter H lessen the produced stresses' amplitude. In terms of stress generation, a comparison analysis reveals that rectangular irregularity is preferable than parabolic irregularity. Additionally, the wave number increases the upper medium's shear and normal stresses. Understanding stress behavior in geophysical structures, subterranean constructions, tunnels, and bridge foundations subjected to movement loads and seismic disturbances may be made easier with the help of the current model. The present study is based on the assumption of a small perturbation parameter (ϵ) and idealized material properties, which may limit its applicability in cases involving large surface irregularities or strongly non-linear material behavior. Furthermore, the proposed model does not account for time-dependent porosity variations, multi-scale interactions, or complex non-linear dynamic effects. Future investigations may extend the present formulation by incorporating non-linear constitutive behavior, advanced dynamic loading conditions, and numerical validation techniques. In addition, more realistic geometrical configurations and multilayered geophysical structures may be considered to improve the applicability of the model in practical geomechanics and structural engineering problems.

Declarations

- The authors received no specific funding for this study.
- The authors declare that they have no conflicts of interest to report regarding the present study.
- No Human subject or animals are involved in the research.
- All authors have mutually consented to participate.
- All the authors have consented the Journal to publish this paper.
- Authors declare that all the data being used in the design and production cum layout of the manuscript is declared in the manuscript.

References

[1] Chonan, S.: Moving load on a pre-stressed plate resting on a fluid half-space. Archive of Applied Mechanics **45**, 171–178 (1976)

[2] Cole, J., Huth, J.: Stresses produced in a half plane by moving loads. Journal of Applied Mechanics **25**, 433–436 (1958)

[3] Craggs, J.W.: One two-dimensional wave in an elastic half plane. Proceedings of the Cambridge Philosophical Society **56**, 269–275 (1960)

[4] Sneddon, I.N.: Stress produced by a pulse of pressure moving along the surface of semi-infinite solid. Rendiconti del Circolo Matematico di Palermo **2**, 57–62 (1952)

[5] Singh, A.K., Kumar, S., Chattopadhyay, A.: Effect of irregularity and heterogeneity on the stresses produced due to a normal moving load on a rough monoclinic half-space. Meccanica **49**(12), 2861–2878 (2014)

[6] Singh, A.K., Mistri, K.C., Chattopadhyay, A.: Normal load moving on magneto-elastic transversely isotropic half space with irregular and hydrostatic initial stress. Journal of Vibration and Control **23**(8), 1354–1373 (2017)

[7] Chatterjee, M., Dhua, S., Chattopadhyay, A.: Response of moving load due to irregularity in slightly compressible, finitely deformed elastic media. Mechanics Research Communications **66**, 49–59 (2015)

[8] Chatterjee, M., Chattopadhyay, A.: Effect of moving load due to irregularity in ice sheet floating on water. Acta Mechanica **228**(5), 1749–1765 (2017)

[9] Chattopadhyay, A., Gupta, S., Sharma, V.K., Kumari, P.: Stresses produced on a rough irregular half-space by a moving load. Acta Mechanica **221**(3–4), 271–280 (2011)

[10] Chattopadhyay, A., Saha, S.: Dynamic response of normal moving load in the plane of symmetry of a monoclinic half-space. Tamkang Journal of Science and Engineering **9**(4), 307–312 (2006)

[11] Chattopadhyay, A., Sahu, S.A.: Stresses produced in slightly compressible, finitely deformed elastic media due to a normal moving load. Archive of Applied Mechanics **82**(5), 699–708 (2012)

[12] Alam, P., Singh, M.K.: Study of love waves in a clamped viscoelastic medium with irregular boundaries. Journal of Solid Mechanics **11**(3), 593–605 (2019)

[13] Sahu, S.A., Singh, M.K., Pankaj, K.K.: Analysis of torsional waves in a prestressed composite structure with loosely bonded and corrugated boundaries. Mechanics of Composite Materials **54**(3), 321–332 (2018)

[14] Mishra, A., Negi, A.: On the dynamic response of a layered heterogeneous rough irregular double porous composite rock structure due to a moving line load. Journal of Engineering Mathematics **150**, 19 (2025)

[15] Dewangan, N., Sahu, S.A., Chaudhary, S.: Dynamic moving load problem in irregular elastic media. Journal of Solid Mechanics **17**, 1–16 (2025)

[16] Singh, M.K., Sahu, S.A., Singhal, A., Chaudhary, S.: Approximation of surface wave velocity in smart composite structure using wentzel–kramers–brillouin method. Journal of Intelligent Material Systems and Structures **29**(18), 3582–3597 (2018)